Degenerate four-wave mixing spectra in a two-level atomic system with phase-modulated time-delayed coherent fields

A. K. Mills
School of Electrical and Computer Engineering, Purdue University, West Lafayette, Indiana 47907, USA

D. S. Elliott
School of Electrical and Computer Engineering and Department of Physics, Purdue University, West Lafayette, Indiana 47907, USA
(Received 23 March 2005; published 12 August 2005)

We study phase-conjugate degenerate four-wave mixing (DFWM) in an optically pumped, two-level atomic system (the $3s\,^2S_{1/2}$, $F=2$, $m_F=2 \rightarrow 3p\,^2P_{3/2}$, $F=3$, $m_F=3$ transition in a diffuse, collision-free, thermal beam of sodium) using phase-modulated laser beams. In this investigation, we study the detailed line shape of the four-wave mixing signal as a function of the temporal delay between the probe field and the pump fields at different intensities of the cw pump waves and modulation frequencies. We show that phase modulation of the pump and probe beams leads to strong amplitude modulation of the phase-conjugate beam and report excellent agreement between our experimental observations of the DFWM spectra and the results of numerical calculations. Our numerical results suggest an enhancement of the "local" DFWM signal when the sidebands of the phase-modulated laser are resonant with dressed-state transitions, but that this resonance is less obvious in the total signal generated. We also show that the complex line shapes depend sensitively upon the delay of the probe beam, with the peak DFWM signal occurring when the probe beam is advanced compared to the pump beam.

DOI: 10.1103/PhysRevA.72.023813 PACS number(s): 42.50.Gy, 32.80.−t, 42.65.Hw

I. INTRODUCTION

In recent studies [1–3] of phase-conjugate degenerate four-wave mixing (DFWM), we have investigated the detailed line shape and signal strength of this important interaction in a closed two-level atomic system. In these works, we drive the atoms with a tunable, narrow-band laser field and reduce the effects of Doppler broadening by carrying out our measurements with an atomic beam. The goal of these studies is to provide measurements that can be used in direct comparison with the fundamental theory of the interaction [4,5] or computational results, and through this to gain a better understanding of its properties. A series of observations [6–24] of this interaction by several groups over the past 25 years has shed a great deal of light on the subject, but the interpretation of these works has, in many cases, been limited by inhomogeneous (Doppler) broadening of the transition, multilevel energy structure of the nonlinear medium, or the use of pulsed lasers that may have operated on multiple modes. In our work, we eliminate or reduce the influence of these factors.

In our previous studies [1,3], we measured the line shapes and signal strengths for phase-conjugate DFWM with a narrow-band laser source and showed excellent quantitative agreement with results we derived from numerical integration of the optical Bloch equations. We also showed that atomic velocity effects were surprisingly strong, even though we used a well-collimated atomic beam in our measurements. Atoms traveling through the standing-wave pattern formed by the counterpropagating pump fields experience a sinusoidally varying field amplitude, and the Bloch vector representing the atomic population and dipole transition amplitude varies in synchronization with this modulation. We have also examined DFWM using randomly-phase-modulated laser fields (known as the phase diffusion field) and observed the influence that these fluctuations can exert on the magnitude and spectrum of the DFWM interaction, as well as the strong dependence of the signal on the temporal delay of the probe with respect to the pump beam [2]. As expected, the DFWM signal decreased with increasing delay, as the correlation between the probe and pump phase decreased. Curiously, the greatest signal occurs when the probe delay is slightly negative—i.e., when the phase fluctuation of the probe beam precedes that of the pump beam.

In the present work, we study a related problem of an atom driven by a set of sinusoidally-phase-modulated laser beams. Similar to the case for the Doppler-shifted atoms discussed above, the Bloch vector of the atomic system responds to the sinusoidally varying field, and the dynamics of this interaction can lead to interesting results. The atomic response, as revealed through the time-dependent DFWM signal, depends sensitively upon the temporal delay between the pump and probe beams. Our experimental observations of this interaction are in excellent agreement with accompanying numerical simulations. An additional manifestation of these dynamics, which we observe in our computational results of the interaction only, is that the maximum DFWM signal occurs for slightly negative probe delays, similar to the randomly-phase-modulated case. In this paper, we describe our measurements, as well as the numerical simulations that help us to understand this complex interaction.

II. EXPERIMENT

In this section we briefly discuss the experimental techniques that we use for measurements of phase-conjugate

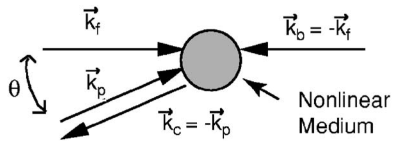

FIG. 1. Wave-vector diagram for the four-wave mixing interaction in the phase-conjugate geometry. Counterpropagating pump beams (propagating in directions $\vec{k}_f$ and $\vec{k}_b=-\vec{k}_f$) and a probe beam ($\vec{k}_p$) interact with the nonlinear medium to produce the phase-conjugate beam ($\vec{k}_c=-\vec{k}_p$).

four-wave mixing spectra. We show a schematic representation of the geometry of the input and output beams in Fig. 1. Three input beams intersect one another in a nonlinear medium (atomic sodium), producing the phase-conjugate beam through their interaction with the medium. The forward and backward pump beams propagate in directions counter to one another (i.e., $\vec{k}_b=-\vec{k}_f$, where $\vec{k}_f$ and $\vec{k}_b$ are the propagation vectors for the forward and backward pump beams) and cross the atomic beam at a right angle. A weak probe beam also crosses the atomic beam at a right angle and propagates at a small angle θ with respect to the forward pump beam. All input laser beams are derived from the same laser source and are at the same frequency. The phase-conjugate beam produced through the DFWM interaction propagates in the direction opposite to that of the input probe beam with $\vec{k}_c=-\vec{k}_p$.

We strive in these measurements to create a highly controlled experimental geometry that yields measurements that are susceptible to direct quantitative comparison with the results of numerical models or analytical expressions of the interaction. To this end, we perform our measurements using (i) a closed, two-level system as the nonlinear medium, (ii) a system with minimal inhomogeneous broadening, (iii) a collision-free system, and (iv) a cw narrow-band optical field. We show a detailed layout of the experiment in Fig. 2. This setup is similar to what we used in previous studies [3], with the added capability of phase modulating the input laser beams. The light source from which all beams are derived is a traveling-wave (ring), stabilized, tunable, cw dye laser operating at 589.0 nm. The linewidth of the laser field is $\Delta\nu_L \sim 200$ kHz. Using beam splitters, an acousto-optic modulator (AOM), and electro-optic modulators, we split the output laser beam into (1) a preparation beam, which optically pumps the sodium atoms into a single hyperfine component ($F=2, m_F=2$) of the ground state [25] (including those that were initially in the $F=1$ ground state) and locks the laser frequency to a controllable value near the atomic transition frequency, (2) the forward and backward pump beams, propagating in directions opposite one another, and (3) the weak probe beam, propagating at a small angle $\theta \sim 1.8°$ with respect to the forward pump beam. All beams are circularly polarized, such that when interacting with the sodium atoms, the laser beams couple the ground state only to the ($3p\ ^2P_{3/2}, F=3, m_F=3$) state, and since the only decay path for these upper state atoms leads to the $F=2$, $m_F=2$ ground state, the atoms behave as a true two-level system. We pass the forward and backward pump beams and the probe beam through lengths of single-mode optical fiber in

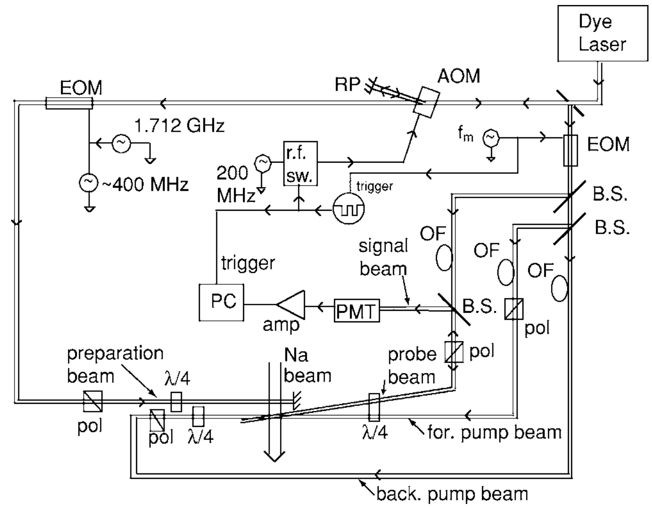

FIG. 2. Schematic diagram for the phase-conjugate four-wave mixing experiment. Abbreviations in this diagram are used for the acousto-optic modulator (AOM), electro-optic modulators (EOM), a roof prism (RP), a rf switch (r.f. sw.), optical beam splitters (B.S.), single-mode optical fibers (OF), the photomultiplier (PMT), a personal computer (PC), polarizers (pol), and quarter-wave retarders (λ/4).

order to improve upon their transverse mode structure. The forward and backward pump beams are characterized by

$$E_{f,b}(t) = E_0 \cos[\vec{k}_{f,b} \cdot \vec{r} - \omega_L t - \phi_0 \cos(2\pi f_m t)], \qquad (1)$$

while the probe beam is

$$E_p(t) = E_p \cos\{\vec{k}_p \cdot \vec{r} - \omega_L t - \phi_0 \cos[2\pi f_m (t-\tau_d)]\}. \qquad (2)$$

ω_L is the radial frequency of the laser field, f_m is the modulation frequency, ϕ_0 is the amplitude of the phase modulation, also known as the modulation parameter, and τ_d is the delay time of the probe beam with respect to the pump beams, which we vary and control by changing the length of the probe beam optical fiber. For all measurements discussed in this study, we use $\phi_0=1$.

In order to keep the atoms in the $3s\ ^2S_{1/2}$, $F=2$, $m_F=2$ state as they travel from the preparation region to the interaction region, we cancel the Earth's magnetic field and apply an additional static field of magnitude ~ 500 mG, oriented parallel to the direction of propagation of the preparation beam. As is standard for interactions with circularly polarized beams, we choose this direction as the quantization axis of our quantum atomic system and denote this the $\hat{z}$ direction.

The pump and probe beams are each in a nearly lowest-order Gaussian mode of radius (defined as the radial distance at which the intensity drops to $1/e^2$ of the on-axis intensity) equal to 1.2 mm and 0.28 mm, respectively. We maintain the ratio of these radii so that the intensity of the pump beam is relatively constant (less than 10% variation) over the dimension of the probe beam. The pump beam intensity is either $7.2I_s^0$ or $28.8I_s^0$, where I_s^0 is the saturation intensity for the transition at the resonance frequency,

$$I_s^0 = \frac{1}{2}\epsilon_0 c \frac{\hbar^2 \gamma_{12}\Gamma_0}{|\mu_{12}|^2}. \tag{3}$$

γ_{12} is the transverse relaxation rate (equal to $\Gamma_0/2$ in the collision-free atomic beam), and μ_{12} is the transition dipole moment. For the transition used in our work, I_s^0 is 6.33 mW cm^{-2}. The powers of the forward and backward pump beams are matched to within 2% of each other. The power of the probe beam is fixed at 2 μW and is actively controlled with an AOM-based amplitude stabilizer. The probe beam intensity at the center of the beam is $I_{\text{probe}}=0.26 I_s^0$ for all measurements. The Rabi frequency of the interaction of the two-level atom with one of the pump beams, $\Omega=\mu_{21}E_0/\hbar=[\gamma_{12}\Gamma_0 I/I_s^0]^{1/2}$, is $2\pi\times 18$ MHz or $2\pi\times 36$ MHz, at the powers used in this work of 1.03 mW or 4.12 mW, respectively. The Rabi frequency of the interaction with the probe beam is $\Omega_p/2\pi=3.6$ MHz.

The phase-conjugate beam propagates backward along the direction of the input probe beam. We separate the phase-conjugate and the input probe beams using a nonpolarizing ~30% beam splitter and direct the former onto the photocathode of a photomultiplier tube [PMT gain=1.9×10^6, with a 8.5% quantum efficiency].

We have described the vacuum system in detail previously [1,3]. The sodium beam is generated by heating a simple stainless-steel effusive oven. The 1.7-mm-diam oven nozzle and a second 1.7-mm aperture 367 mm away define the collimated atomic beam in the interaction region. At an oven temperature of 290 °C(±5 °C), as we use in our experiment, the beam density in the interaction region is 2×10^8 cm^{-3} and the root-mean-square velocity of the atoms is $\langle v\rangle_{\text{rms}}=9\times 10^4$ cm/sec. We measure weak field absorption spectra daily and observe a typical linewidth of 13–14 MHz, only slightly greater than the 10-MHz natural linewidth of the transition. We fit these absorption spectra to a Voight profile, assuming a Gaussian distribution of atomic velocities in the direction of the laser propagation vector $\vec{k}_f$,

$$P(v_z) = \sqrt{\frac{4\ln 2}{\pi}}\frac{1}{\Delta v_z}\exp\left[-4\ln 2\left(\frac{v_z - v_{z0}}{\Delta v_z}\right)^2\right], \tag{4}$$

where v_{z0} is the (small) average velocity in the $\hat{z}$ direction, which could be nonzero due to imperfect alignment of the laser beams, and Δv_z is the width of the velocity distribution. v_{z0} is typically on the order of ±20 cm/s, corresponding to a laser misalignment of ±0.2 mrad, while Δv_z is typically 500–600 cm/s. The peak attenuation factor $2\alpha_0 L$ is typically 0.07–0.08, where α_0 is the field attenuation constant for stationary atoms,

$$\alpha_0 = \frac{\pi \nu_L N |\mu_{12}|^2}{c\hbar\epsilon_0\gamma_{12}}. \tag{5}$$

N is the atomic beam density and L is the absorption length—i.e., the diameter of the atomic beam.

In order to eliminate effects due to the velocity of the atoms changing as they absorb light from the forward and backward pump beams before they reach the probe beam [3], we chop the probe and pump beams by controlling the amplitude of the rf signal that drives the AOM. This allows us

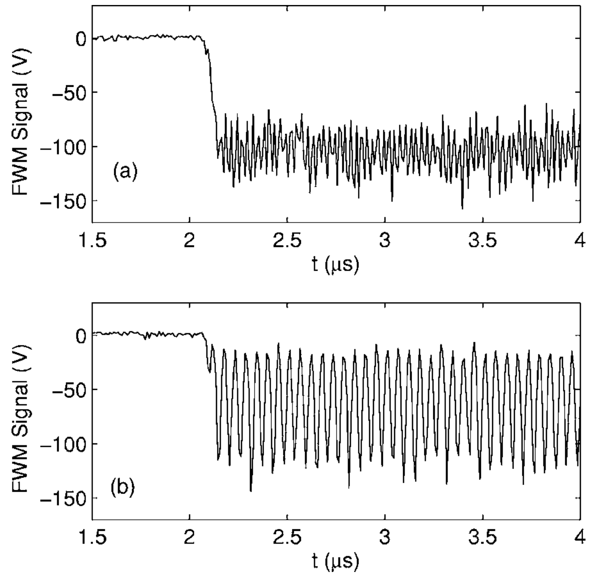

FIG. 3. The oscilloscope trace of the DFWM signal corresponding to the accumulated signal (5000 wave forms) for (a) $\delta=0$ and (b) $\delta=-2\pi\times 18$ MHz. The pump and probe beams turn on at about $t=2$ μs. In each case the Rabi frequency of the interaction with a single pump beam is 18 MHz and the modulation frequency is $f_m=18$ MHz.

to observe the DFWM signal before the atomic velocities are significantly modified. The period of the cycle is 20 μs, its duty cycle is 50%, and we synchronize the time at which the laser beams turn on with the modulation of the phase. During the 10-μs interval during which the pump and probe beams are off, the atoms completely traverse the pump beam region. We then repeat the cycle with a fresh group of atoms.

We amplify, display, and record the photomultiplier current with an electronic amplifier (gain=650, input impedance=50 Ω, bandwidth=0–50 MHz) and a digitizing plug-in card (100 MS/s sampling rate, input impedance =50 Ω, bandwidth=0–100 MHz) in a laboratory PC. The DFWM signal is so weak that we detect only a few DFWM photons, each appearing as a short (15–20 ns) pulse of mean amplitude ~−600 mV, during a single cycle of the measurement. By accumulating the signal over 5000 wave forms, however, we are able to obtain signals such as those shown in Fig. 3. The pump and probe beams turn on at about $t=2$ μs. In Fig. 3(a) the detuning of the pump and probe beam frequency from the atomic resonance frequency ω_a is $\delta=\omega_L-\omega_a=0$, while in (b) $\delta=-2\pi\times 18$ MHz. In each case the Rabi frequency of the interaction of the atom with a single pump field is 18 MHz and the modulation frequency is $f_m=18$ MHz. In the zero-detuning case, the modulation of the DFWM signal is relatively weak and the primary frequency is $2f_m$. In (b), the amplitude modulation of the signal is very strong and primarily at the modulation frequency f_m. By contrast, the DFWM signal in the absence of phase modulation of the input field shows no amplitude modulation, as shown in Fig. 3 of Ref. [3].

In our analysis of these data, we limit our attention to the period starting at about 2.50 μs and lasting for about 280 ns, in order to reduce the influence of the atomic recoil on our

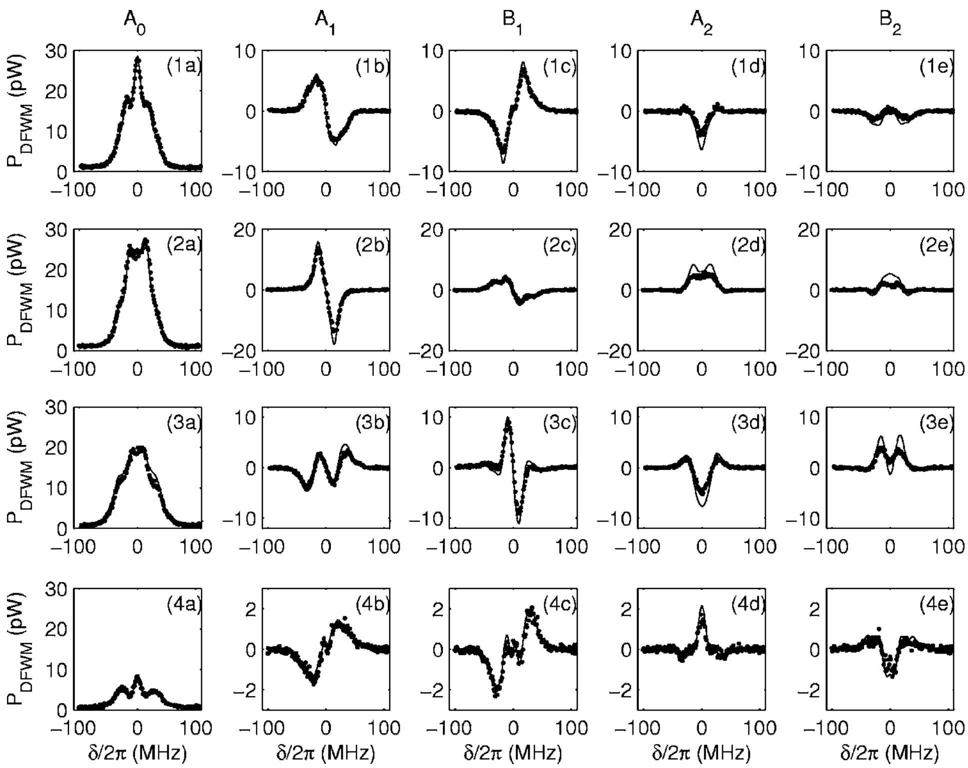

FIG. 4. The spectra of the DFWM signal: (1a–1e) zero delay of the probe beam with respect to the pump beam, (2a–2e) $\tau_d = -T_m/4$, (3a–3e) $\tau_d = -T_m/2$, and (4a–4e) $\tau_d = -3T_m/4$. The spectra in the five columns correspond to (1a–4a) the mean DFWM signal, (1b–4b) the amplitude of the in-phase component of the sinusoidal modulation of the DFWM signal at frequency f_m, (1c–4c) the amplitude of the quadrature-phase component at frequency f_m, (1d–4d) the amplitude of the in-phase component of the sinusoidal modulation of the DFWM signal at frequency $2f_m$, and (1e–4e) the amplitude of the quadrature-phase component at frequency $2f_m$. In each case the Rabi frequency of the interaction is 18 MHz and the modulation frequency is $f_m = 18$ MHz.

DFWM spectra. We scan the laser over a ±100 MHz range about the sodium resonant frequency and record the time-dependent data at ~200 laser detunings over a 20-min scan. We correct the data to account for spontaneous emission originating from the excited-state sodium atoms in the interaction region by repeating the measurement with the probe beam blocked. We fit the spontaneous emission spectrum to a form consisting of three Lorentzian functions (spaced by f_m) and subtract this function from the measured DFWM spectrum. The magnitude of this spontaneous emission signal was relatively constant for each of the DFWM measurements reported in this work. For the stronger DFWM signals, the spontaneous emission background was only about 10% of the signal. While the spontaneous emission background actually exceeded the signal for the cases where the DFWM signal was weaker, the uncertainty in the DFWM data appears to be satisfactory for all cases.

III. RESULTS AND DISCUSSION

We measured and recorded degenerate four-wave mixing spectra at three combinations of Rabi frequency and modulation frequency, and determine the amplitude and phase of the modulated DFWM signal by performing a Fourier decomposition of time-dependent wave forms like those shown in Fig. 3. We write the optical power of the DFWM signal as

$$P_{\mathrm{DFWM}}(t) = A_0 + \sum_{n=1}^{2} A_n \cos[2\pi n f_m t - n\phi'] + B_n \sin[2\pi n f_m t - n\phi']. \quad (6)$$

The phase ϕ' accounts for the difference in turn-on time between theoretical (to be discussed next) and experimental DFWM signals.

In Fig. 4, we show DFWM data corresponding to a Rabi frequency $\Omega/2\pi$ of 18 MHz and a modulation frequency of $f_m = 18$ MHz. The data points in this figure correspond to the average DFWM power and the amplitudes of sinusoidally varying components. The data points in the plots within column *a* represent the average DFWM signal (A_0), in columns *b* and *c* the in-phase (A_1) and quadrature-phase (B_1) amplitudes at frequency f_m, and columns *d* and *e* the in-phase (A_2) and quadrature-phase (B_2) amplitudes at frequency $2f_m$. The four rows correspond to varying delay of the probe beam with respect to the pump beam τ_d. In the top row (1a–1e), the probe delay is $\tau_d = 0$. In the second, third, and fourth rows, the probe beam is advanced (i.e., $\tau_d < 0$) by $T_m/4$, $T_m/2$, and $3T_m/4$, respectively, where $T_m = 1/f_m$ is the period of the modulation. (We choose to advance the probe beam to avoid recoil effects that would occur if the pump beams turn on before the probe beam.) The mean DFWM signal shows a series of not-quite-resolved peaks at detunings from resonance of zero and close to integer multiples of f_m. When one considers the power spectrum of the phase-modulated laser field, consisting of the carrier at frequency $\omega_L/2\pi$ and sidebands to either side spaced by f_m, this result is not surprising, since we would reasonably expect a peak in the DFWM signal when the carrier or a sideband is resonant with the atomic transition frequency.

The variation among these spectra as we delay the probe beam is striking. At zero delay, the mean DFWM spectrum shows a large central peak and two smaller sidebands at the modulation frequency f_m. Advancing the probe beam by a quarter period ($\tau_d = -T_m/4$) elevates the sidebands so that they are stronger than the central peak. An additional ad-

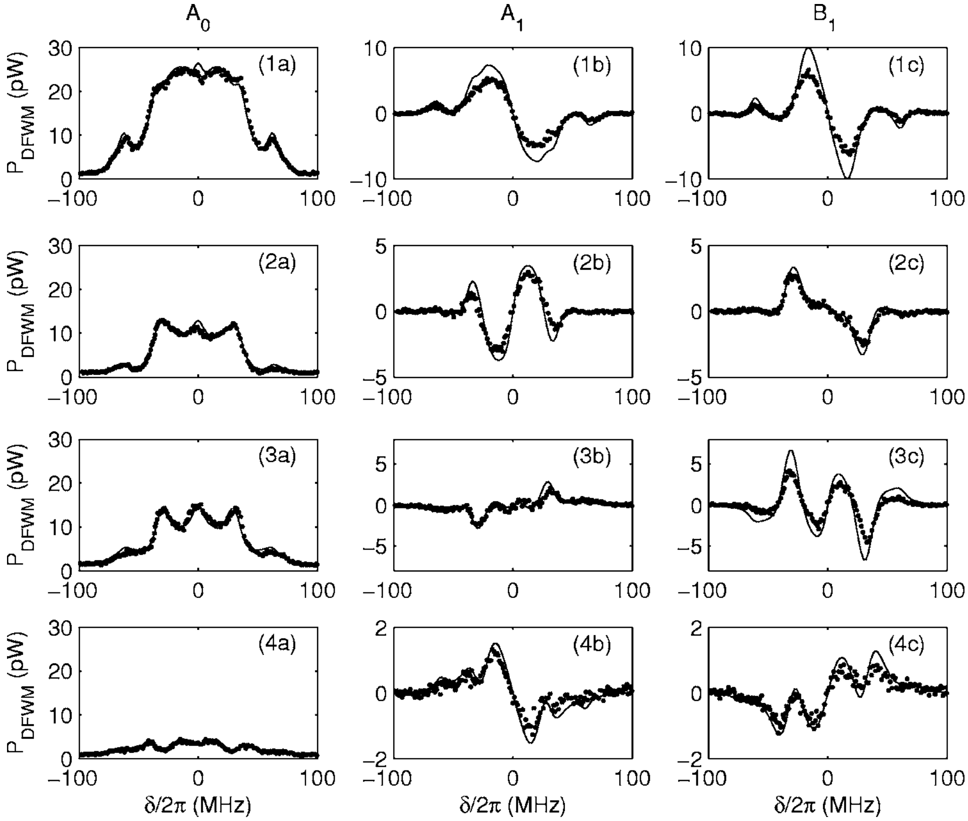

FIG. 5. The spectra of the DFWM signal for the case when the Rabi frequency of the interaction is 18 MHz and the modulation frequency is f_m=36 MHz. All spectra are as identified in the caption to Fig. 4.

vance to $\tau_d=-T_m/2$ shows evidence of sidebands at $2f_m$, and finally the sidebands at f_m in the $-3T_m/4$ delay are almost completely absent, while those at $2f_m$ are strong. The peak signal at a delay of $-3T_m/4$ is only about 1/5 the zero delay signal. The amplitude of the oscillating part of the DFWM spectra undergoes similar rapid variation as a function of delay. In each case the amplitude of the modulation at frequency f_m goes to zero at detuning $\delta=0$, as expected from analogous optical interactions with phase modulated light [26], while the $2f_m$ component is peaked. The qualitative picture for this is that as the laser frequency modulates about the peak of the resonance, the atomic dipole goes through two cycles for each cycle of the optical phase. (The atomic response decreases to one side of resonance, returns at the peak, decreases to the other side of resonance, and returns again to the peak.) Thus the amplitudes A_1 and B_1 are odd functions of δ in each case, while the amplitudes A_2 and B_2 are even functions of detuning.

For comparison with these experimental data, we show in Fig. 4 numerical results for the average DFWM signal and the amplitude of the sinusoidal modulation of the DFWM signal as solid lines. We use the theoretical approach described in Ref. [3]. This approach uses the optical Bloch equations to describe the time evolution of the elements of the density matrix of the atomic two-level system and is very similar to that used by Lucht *et al.* [19]. When the intensity of the probe beam is much less than the saturation intensity for the transition, but that of the pump beams is arbitrary, we can expand the coherence term $\sigma_{21}(\vec{r},t)=\rho_{21}(\vec{r},t)e^{i\omega_L t}$ and the population probability difference $W(\vec{r},t)=\rho_{22}-\rho_{11}$ in a power series in the phase term of the probe field,

$$\sigma_{21}(\vec{r},t) = \sigma_{21}^{(0)}(\vec{r},t) + \sigma_{21}^{(1)}(\vec{r},t)e^{i\vec{k}_p\cdot(\vec{r}+\vec{v}t)} + \sigma_{21}^{(-1)}(\vec{r},t)e^{-i\vec{k}_p\cdot(\vec{r}+\vec{v}t)}$$

$$W(\vec{r},t) = W^{(0)}(\vec{r},t) + W^{(1)}(\vec{r},t)e^{i\vec{k}_p\cdot(\vec{r}+\vec{v}t)} + W^{(-1)}(\vec{r},t)e^{-i\vec{k}_p\cdot(\vec{r}+\vec{v}t)}. \tag{7}$$

The component $\sigma_{21}^{(-1)}(r,t)$ is the complex amplitude of the element of the dipole term that radiates the phase conjugate field. The real (imaginary) component of this amplitude describes the component of the dipole that is in phase with (in quadrature to) the oscillating electric field of the pump and probe beams. This expansion, after being substituted into the Bloch equations, yields a set of six coupled equations for the coherence and population difference terms, as given by Eqs. (16) of Ref. [3]. We numerically integrate these equations, starting with the initial conditions of $W^{(0)}=-1$ and all other terms equal to 0 (i.e., the entire population is in the ground state initially). In the present case with phase-modulated pump and probe fields, the Rabi frequency of the interaction of the two-level atom with one of the pump beams and the Rabi frequency for the probe beam interaction include a sinusoidally varying phase, with a phase shift of $2\pi f_m \tau_d$ between them. After a brief transient response of the atomic Bloch vector due to the fields turning on, each of the coherence amplitudes $\sigma_{21}^{(-1)}$, $\sigma_{21}^{(0)}$, and $\sigma_{21}^{(+1)}$ and each of the population amplitudes $W^{(-1)}$, $W^{(0)}$, and $W^{(+1)}$ settles into a steady-state behavior consisting of a dc term and terms oscillating at the frequency f_m and its harmonics. To compute the net phase-conjugate amplitude, we integrate over the standing-wave pattern of the pump beams to include the contribution of all the atoms radiating into this beam throughout the in-

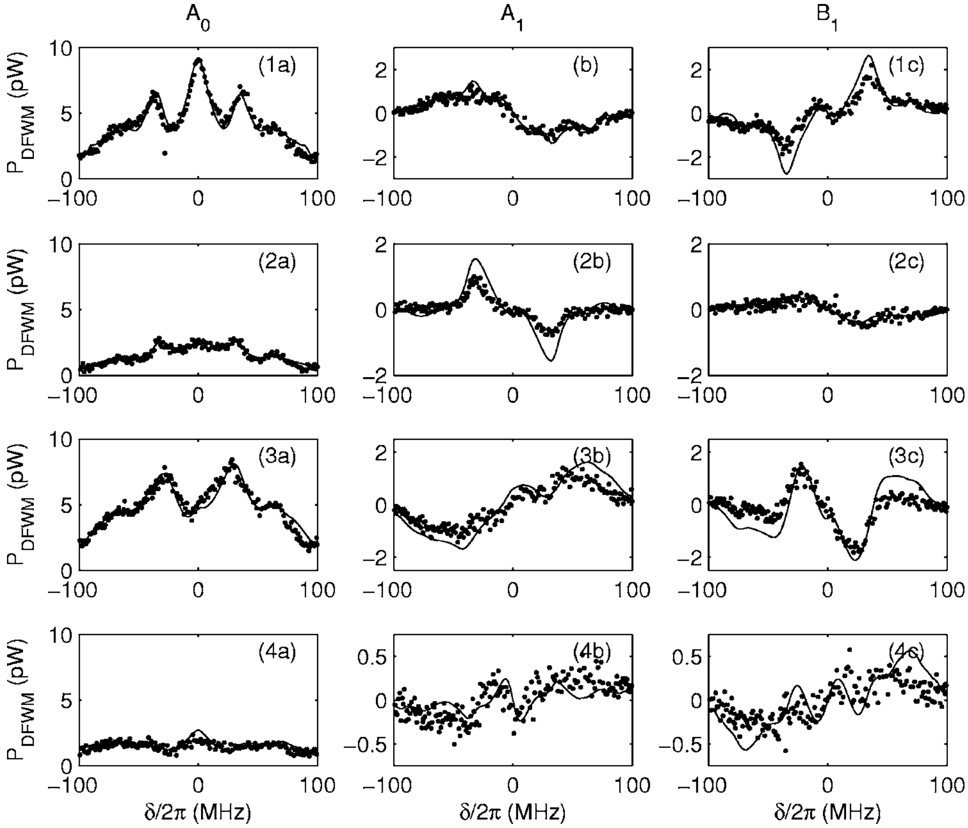

FIG. 6. The spectra of the DFWM signal for the case when the Rabi frequency of the interaction is 36 MHz and the modulation frequency is f_m=36 MHz. All spectra are as identified in the caption to Fig. 4.

teraction region and average over the complex time-dependent DFWM field amplitudes computed for different values of the atomic velocity, weighted by the probability distribution given in Eq. (4). We calculate the optical power of the DFWM beam using [1]

$$P_{\mathrm{DFWM}} = C\left|2\alpha_0 L\frac{\gamma_{12}}{\Omega_p}\langle\sigma_{21}^{(-1)}\rangle\right|^2 P_p, \tag{8}$$

where P_p is the power of the probe beam. The only parameters that we adjust in order to optimize the agreement of the computed spectra with the measured spectra are C, a multiplicative scaling factor of order unity (actual values range between 0.6 and 1.8), the reference phase ϕ' introduced in Eq. (6), and v_{z0}. We adjust the scaling factor to yield good agreement with the mean DFWM signal (A_0) only and find that this yields good agreement for the amplitudes of the sinusoidal components as well. In adjusting ϕ', one value is sufficient to yield good agreement for all four sinusoidal components. We adjust v_{z0} to match the small asymmetry of the spectra. All adjustments of v_{z0} were within the experimental uncertainty of the absorption measurement, as DFWM measurements are much more sensitive to this parameter. The small deviations between our measured values of A_2 and B_2 and the numerical results are likely due to the limited bandwidth of our detection system.

We also collect data at other Rabi frequencies and/or modulation frequencies and show these spectra in Figs. 5 and 6. In Fig. 5, the Rabi frequency for a single pump beam is 18 MHz, while in Fig. 6, the Rabi frequency is increased to 36 MHz. The modulation frequency is 36 MHz for both these figures. We do not include data for the amplitudes of the second-harmonic frequency $2f_m$ in these figures, since this frequency is outside the detection bandwidth of our instrumentation. Again, these spectra are marked by strong features in the mean DFWM signal, the in-phase, and the quadrature-phase amplitudes of the oscillating term. We observe very strong variation of these spectra with delay. Again we attribute the slight difference between experimental and computational results to the limited bandwidth of our detection system.

The effects of atomic velocity on the DFWM spectra are significant even in the atomic beam used in our experiments. The Doppler shifts tend to obscure many of the fine features of the phase-modulated spectrum. The degree to which the atomic velocity alters the overall DFWM spectrum also varies with probe delay. We find this to be particularly evident in the half-modulation period delay cases, where the spectra for the zero velocity and Doppler broadened spectra are vastly different. These experimentally unavoidable effects complicate the formulation of a simplified picture of the DFWM interaction, and we are left to explore the interaction numerically in pursuit of this goal.

In light of the very good agreement between the measured DFWM spectra and computational results, we have gained sufficient confidence in the numerical results that we can use them to examine several fundamental questions concerning the four-wave mixing interaction. Our goal is to develop a simple intuitive picture of the interaction that will afford us better insight into its essential properties and aid in its application to other problems of interest. We would also like to understand (1) if it is possible to identify any range of loca-

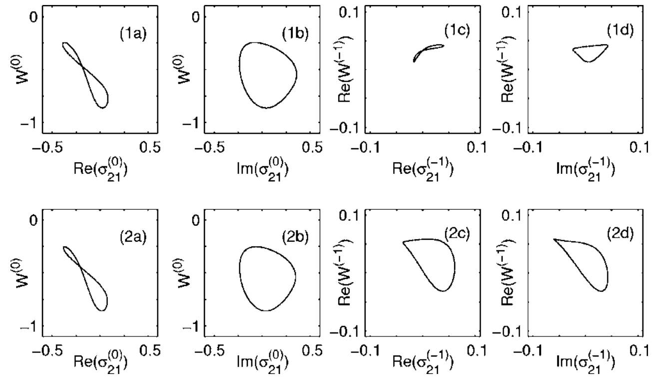

FIG. 7. Trajectories of the components of the Bloch vector at $z=\lambda/16$. The Rabi frequency for these figures is $\Omega/2\pi=18$ MHz, and the detuning of the laser field frequency from the atomic frequency is $\delta/2\pi=18$ MHz. In (1a)–(1d) the delay of the probe field with respect to the pump field is $\tau_d=T_m/4=13.9$ ns, while for (2a)–(2d) is $\tau_d=-13.9$ ns. In each case, the time required to follow the trajectory through one cycle is T_m.

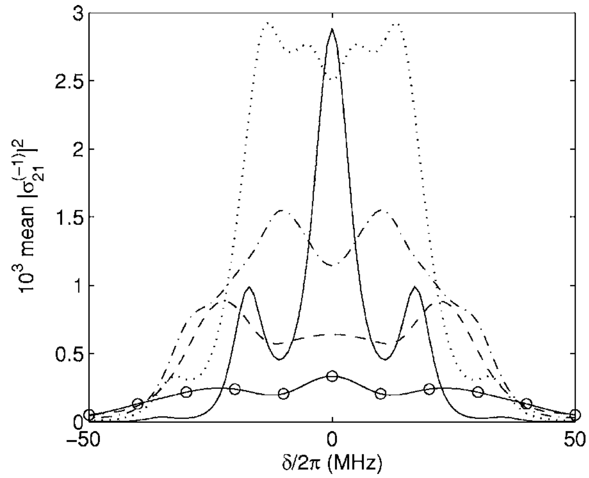

FIG. 8. The mean value of $|\sigma_{21}^{(-1)}|^2$ as a function of δ at five locations within the standing-wave pattern: $z=\lambda/32$ (solid line), $\lambda/16$ (dotted line), $3\lambda/32$ (dot-dashed line), $\lambda/8$ (dashed line), and $\lambda/4$ (solid line with circles), where the node of the standing-wave pattern is at $z=0$.

tions within the standing-wave pattern of the pump beams from which the contribution to the DFWM signal dominates, (2) the role of the Rabi frequency, and (3) the value of τ_d at which the DFWM signal is maximum. In the following, we discuss some of our observations and findings.

For a simple two-level atom interacting with a single, monochromatic laser field, the trajectory of the Bloch vector has been known to yield a simple intuitive picture that allows easy visualization of the temporal response of the atomic population and oscillating dipole moment as the system is driven by the field [27]. In an effort to extend this intuitive, geometrical picture to the DFWM interaction, we have carried out a series of calculations of the trajectories of the components of the Bloch vector. While such an analysis in the present system provides us with some insight into the DFWM interaction, we shall show here that its utility is not nearly as great as it is for a single-frequency interaction. The major shortcoming in the present case is that the optical field, and therefore the Bloch vector of the atomic system, varies within the interaction region on the scale of the wavelength of the light. We therefore need to evaluate the temporal dependence of the system at various locations throughout the interaction region. In addition, the component of the oscillating dipole moment that is phase matched to radiate into the backward direction, $\sigma_{21}^{(-1)}$, is small in comparison to the first-order, non-phase-matched term $\sigma_{21}^{(0)}$. In Fig. 7 we show two such sets of trajectories. The Rabi frequency for these figures is $\Omega/2\pi=18$ MHz, and the detuning of the laser field frequency from the atomic frequency is $\delta/2\pi=18$ MHz. The atom is located a distance $\lambda/16$ from a node of the standing-wave pattern of the pump field. In panels (1a)–(1d) of this figure the delay of the probe field with respect to the pump field is $\tau_d=T_m/4=13.9$ ns, while for (2a)–(2d) is $\tau_d=-13.9$ ns. There are several observations one can make by studying trajectories like those pictured here. First, the trajectories of $W^{(0)}$ vs $\sigma_{21}^{(0)}$ are relatively independent of the probe delay time. This is not surprising in that the evolution of these components is controlled largely by the forward and backward pump fields, and depends very little on the probe beam. These components, however, have only an indirect effect on the phase conjugate field. The $\sigma_{21}^{(-1)}$ term, which radiates the phase-conjugate field, shows a strong dependence on the delay time and shows a very different behavior for positive or negative delay. Note the very different trajectory in Figs. 7(1c) and 7(1d) from that in Figs. 7(2c) and 7(2d). The trajectories at different locations within the standing-wave pattern are also revealing in that they vary greatly as we move through the standing-wave pattern formed by the pump beams. The trajectories show a left-right symmetry only for the case $\delta=0$. For $\delta\neq 0$, the trajectories for $\mathrm{Im}(\sigma_{21}^{(0)})$ or $\mathrm{Im}(\sigma_{21}^{(-1)})$ do not change upon $\delta\to-\delta$, while those for the real part are reversed. Another general trend can be seen in the average magnitude of $W^{(0)}$ as we move through the standing-wave pattern. As expected, the average magnitude of $W^{(0)}$ grows from -1 at the node to a value approaching zero (i.e., the average population is evenly distributed between the upper and lower states) at the antinode. It is interesting that $W^{(0)}$ can exceed zero (a population inversion) for short periods of time during its trajectory.

Since the trajectories vary so greatly over the standing-wave pattern, it would be of great utility if it were possible to identify a limited range of locations within the standing-wave pattern that contributes more significantly to the DFWM signal than others. If valid, this could significantly simplify our picture of the interaction, in that we could focus our attention on that location and ignore elsewhere. In Fig. 8 we show the mean value of $|\sigma_{21}^{(-1)}|^2$ as a function of δ at five locations within the standing-wave pattern: $z=\lambda/32$ (solid line), $\lambda/16$ (dotted line), $3\lambda/32$ (dot-dashed line), $\lambda/8$ (dashed line), and $\lambda/4$ (solid line with circles), where the node of the standing-wave pattern is at $z=0$ and the antinode at $z=\lambda/4$. For the solid-line curve, for which $z=\lambda/32$, the "local" Rabi frequency of this interaction is $\Omega_{\mathrm{local}}/2\pi=7.0$ MHz, somewhat less than, but still comparable to, $\Gamma_0/2\pi=10$ MHz. We define Ω_{local} as $2\Omega\sin(kz)$. This curve shows a strong central peak, with well-resolved sidebands at

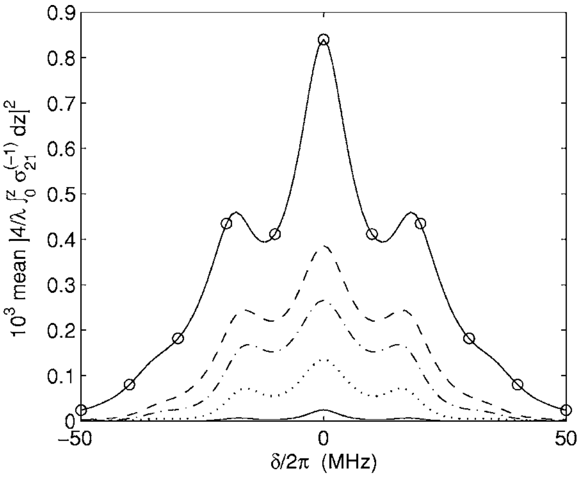

FIG. 9. Calculated results for the integrated DFWM signal that is generated in the region between $z=0$ (the node of the field pattern) and $z=\lambda/32$ (solid line), $\lambda/16$ (dotted line), $3\lambda/32$ (dot-dashed line), $\lambda/8$ (dashed line), and $\lambda/4$ (solid line with circles).

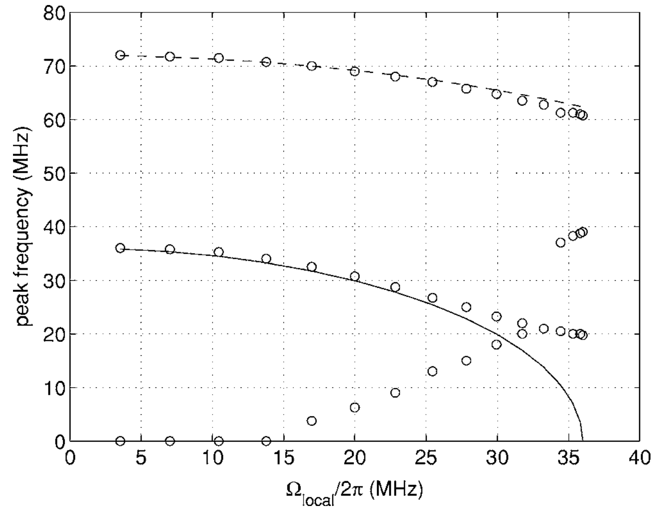

FIG. 10. The frequencies of the peaks in the calculated spectra of the mean value of $|\sigma_{21}^{(-1)}|^2$ vs the local value of the Rabi frequency. The solid line is a plot of $[f_m^2-(\Omega_{\mathrm{local}}/2\pi)^2]^{1/2}$, and $[(2f_m)^2-(\Omega_{\mathrm{local}}/2\pi)^2]^{1/2}$ is shown as a dashed line. These data correspond to calculated DFWM spectra for $\Omega/2\pi=18$ MHz and $f_m=36$ MHz.

nearly f_m to either side. Small peaks at $\sim 2f_m$ can also be observed. Moving to $z=\lambda/16$ (dotted line), the local Rabi frequency has increased to 13.8 MHz, and the line shape has evolved rapidly to one with strongly overlapping peaks and barely distinguishable local maxima at 5 MHz, 13 MHz, and 32 MHz. The amplitude of this peak is slightly greater than the curve at $z=\lambda/16$. The DFWM curves continue to evolve rapidly for locations at greater distances from the node, but now one can see a decrease in amplitude as well. The local Rabi frequency is 20.0 MHz, 25.5 MHz, and 36.0 MHz, for the curves at $z=3\lambda/32$, $\lambda/8$, and $\lambda/4$, respectively. This is consistent with prior works [4] that concluded that the major contributions to the net DFWM signal are derived from the region within the standing-wave pattern where the interaction is nearly saturated; i.e., the local Rabi frequency is comparable to Γ_0. If the intensity of the two pump beams is very large, this can be a very narrow region. It does not appear, however, that this is sufficient to simplify the analysis of the interaction, because of the rapid variation of $\sigma_{21}^{(-1)}$ as a function of Ω_{local}. In addition, while $|\sigma_{21}^{(-1)}|^2$ does, in fact, decrease for $z>\lambda/16$, the dipoles in the region $\lambda/16<z<\lambda/4$ still contribute significantly to the signal due to the large size of this space. We illustrate this in Fig. 9, where we plot $|4/\lambda\int_0^z\sigma_{21}^{(-1)}dz|^2$, for $z=\lambda/32$ (solid line), $\lambda/16$ (dotted line), $3\lambda/32$ (dot-dashed line), $\lambda/8$ (dashed line), and $\lambda/4$ (solid line with circles). This integral represents the DFWM signal as we integrate over an increasing fraction of the standing-wave pattern of the pump beams, and we observe that the DFWM spectrum continues to grow over this entire range.

In addition to variations in the magnitude of $|\sigma_{21}^{(-1)}|^2$ with location, the frequency at which the peaks occur can also be seen to vary. This appears to be due to a resonance enhancement effect as the laser sidebands come into resonance with transitions between dressed states of the atom. Resonant enhancement in four-wave mixing has been discussed in several contexts previously. In a series of papers, Grynberg, Pinard, and Verkerk [8,10,11] studied nondegenerate four-wave mixing interactions in neon for the case when only one pump beam was intense. The measured and calculated spectra in this case showed peaks separated by the Rabi frequency of the interaction of the atom with the intense pump beam. Lin, Rubiera, and Zhu [12] observed nondegenerate four-wave mixing in rubidium and reported structure in their spectra at the Rabi frequency as well. While the intensities of both of their pump beams exceeded the saturation intensity for the transition, one beam was much more intense than the other, decreasing the variation of the local Rabi frequency across the standing-wave pattern of the pump beams. In the case of degenerate four-wave mixing in the phase-conjugate geometry with equal-intensity pump beams, however, the situation is quite different, and one should not expect to observe any strong signatures of the Rabi frequency in the four-wave mixing spectra. As we illustrate here, local enhancement is possible, but these features do not survive in the net signal. In Fig. 10 we plot the frequencies δ at which peaks occur in the local DFWM spectra, similar to the one shown in Fig. 8, as a function of the local Rabi frequency. The peak frequencies in this figure, corresponding to $\Omega/2\pi=18$ MHz and $f_m=36$ MHz, appear as three series: one that starts as a central peak for small Ω_{local}, one that starts at f_m, and one that starts at $2f_m$. The former is also present in calculated spectra for a monochromatic laser field (i.e., $\phi_0=0$) and therefore is unrelated to the optical sidebands. For the other two series, the frequencies of the local maxima in the DFWM signal can be seen to decrease as Ω_{local} increases. This is consistent with a picture of the interaction in which one of the optical sidebands at frequency $\omega_L \pm 2n\pi f_m$ is resonant with a transition between dressed-state levels of the atom at frequency $\omega_L \pm \Omega'$, where n is an integer and Ω' is the generalized Rabi frequency of the interaction, equal to $[\delta^2+\Omega_{\mathrm{local}}^2]^{1/2}$. We have plotted $[f_m^2-(\Omega_{\mathrm{local}}/2\pi)^2]^{1/2}$ (solid line) and $[(2f_m)^2-(\Omega_{\mathrm{local}}/2\pi)^2]^{1/2}$ (dashed line) in the figure,

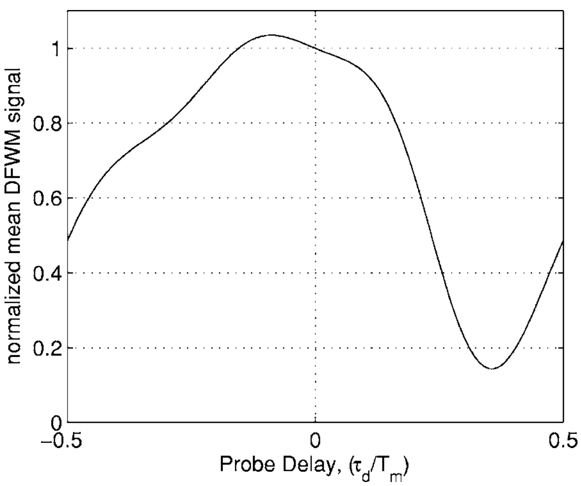

FIG. 11. The normalized DFWM signal at zero detuning as a function of the delay between the pump and probe beams, τ_d. The Rabi frequency of the interaction is 18 MHz and the modulation frequency is $f_m = 18$ MHz, and all atoms are considered to be at rest.

corresponding to the dressed levels of the atom-field system, valid for an interaction with a single-frequency pump field. While the dressed-state resonances for an atom in a trichromatic field will be somewhat different from these curves, the correspondence at low values of Ω_{local} indicates that the peaks in the DFWM signal occur when the sidebands of the phase-modulated input fields are resonant with transitions between dressed atom levels. This picture is complicated for larger Ω_{local}, because the laser sidebands can also saturate the transition. These features appear in plots of the *local* values of $|\sigma_{21}^{(-1)}|^2$ only. The *net* signal includes contributions from atoms distributed throughout the interaction region, and signatures of local Rabi frequencies become difficult to identify.

Finally, we have examined the dependence of the four-wave mixing signal on the temporal delay between the pump and probe fields. In previous studies of phase-conjugate DFWM with randomly-phase-modulated fields, the phase diffusion field [2], we showed that the maximum signal resulted when the probe beam was slightly advanced with respect to the pump beam—i.e., when τ_d was slightly negative. Our numerical studies show similarly that the DFWM signal in the present case is greatest for negative τ_d. We show this dependence in Fig. 11. Unlike the phase diffusion field, the DFWM signal is periodic in τ_d. We generated this curve assuming all the atoms are stationary, so we do not show experimental data in this figure. Still, we note reasonable qualitative agreement with the relative magnitudes of the DFWM signals in Figs. 4(1a)–4(4a), especially considering the variations in the laser beam alignment and atom beam density that must invariably be present between measurements. We did not attempt to tune the delay time to the optimal value.

IV. CONCLUSIONS

In this work, we have presented our experimental measurements of phase-conjugate four-wave mixing spectra for a system of two-level atoms interacting with a phase-modulated laser beam. In general, we observe strong amplitude modulation of the DFWM signal at the phase-modulation frequency of the pump and probe fields and its second-harmonic frequency. As we vary the Rabi frequency of the interaction, the modulation frequency, or the delay time between the pump and probe beams, we observe very strong variation of the DFWM spectra. These experimental measurements are in very good agreement with numerical results, which we derive through numerical integration of the optical Bloch equations. As was the case in our previous measurements of four-wave mixing interactions, the effect of Doppler shifts due to the velocity of the atoms is critical, even in our case of an atomic beam with reasonably good collimation. Throughout this work, one of our outstanding goals has been to develop a simple picture of the interaction. There are, of course, a few notable successes to this, as we have tried to point out in the preceding descriptions. There have also been some notable challenges to this attempt. The major roadblock to forming this simple picture stems from two factors. First, the DFWM signal is generated by only one component of the coherence term σ_{21}—i.e., the term that is phase matched to radiate into the conjugate beam. This component of σ_{21} is only a minor part of the whole coherence term. In addition, since the Rabi frequency of the interaction varies sinusoidally over the interaction region, the magnitude and phase of σ_{21} vary significantly over this range. Because of these complications to the interaction, our efforts to form a simple picture have been only partially successful.

ACKNOWLEDGMENTS

We gratefully acknowledge the important suggestions of P. Berman and the advice and critical technical input of Binh Do. One of us (A.K.M.) also acknowledges support through the Graduate Assistance in Areas of National Need program of the Department of Education.

[1] Binh Do, Jongwhan Cha, D. S. Elliott, and S. J. Smith, Phys. Rev. A **58**, 3089 (1998).
[2] Binh Do, Jongwhan Cha, D. S. Elliott, and S. J. Smith, Phys. Rev. A **60**, 508 (1999).
[3] Binh Do and D. S. Elliott, Phys. Rev. A **67**, 063810 (2003).
[4] R. L. Abrams and R. C. Lind, Opt. Lett. **2**, 94 (1978); **3**, 205 (1978).
[5] R. L. Abrams, J. F. Lam, R. C. Lind, D. G. Steel, and P. F. Liao, in *Optical Phase Conjugation*, edited by Robert A. Fisher (Academic Press, San Diego, 1983), Chap. 8.
[6] P. F. Liao, D. M. Bloom, and N. P. Economou, Appl. Phys. Lett. **32**, 813 (1978).
[7] D. Bloch, R. K. Raj, K. S. Peng, and M. Ducloy, Phys. Rev. Lett. **49**, 719 (1982).

[8] G. Grynberg, M. Pinard, and P. Verkerk, Opt. Commun. **50**, 261 (1984).
[9] M. Ducloy, F. A. M. de Oliveira, and D. Bloch, Phys. Rev. A **32**, 1614 (1985).
[10] P. Verkerk, M. Pinard, and G. Grynberg, Phys. Rev. A **34**, 4008 (1986).
[11] M. Pinard, P. Verkerk, and G. Grynberg, Phys. Rev. A **35**, 4679 (1987).
[12] J. Lin, A. I. Rubiera, and Y. Zhu, Phys. Rev. A **52**, 4882 (1995).
[13] M. Oria, D. Bloch, M. Fichet, and M. Ducloy, Opt. Lett. **14**, 1082 (1989).
[14] S. M. Wandzura, Opt. Lett. **4**, 208 (1979).
[15] D. G. Steel, R. C. Lind, J. F. Lam, and C. R. Guiliano, Appl. Phys. Lett. **35**, 376 (1979).
[16] L. M. Humphrey, J. P. Gordon, and P. F. Liao, Opt. Lett. **5**, 56 (1980).
[17] D. G. Steel and J. F. Lam, Opt. Commun. **40**, 77 (1981).
[18] P. R. Berman, D. G. Steel, G. Khitrova, and J. Liu, Phys. Rev. A **38**, 252 (1988).
[19] R. P. Lucht, R. L. Farrow, and D. J. Rakestraw, J. Opt. Soc. Am. B **10**, 1508 (1993).
[20] D. S. Glassner, B. Ai, and R. J. Knize, Opt. Lett. **19**, 2071 (1994).
[21] D. J. Harter and R. W. Boyd, Phys. Rev. A **29**, 739 (1984).
[22] G. C. Cardoso and J. W. R. Tabosa, Opt. Commun. **185**, 353 (2000).
[23] A. Lezama, G. C. Cardoso, and J. W. R. Tabosa, Phys. Rev. A **63**, 013805 (2000).
[24] S. Barreiro and J. W. R. Tabosa, Opt. Commun. **233**, 383 (2004).
[25] R. E. Grove, F. Y. Wu, and S. Ezekiel, Phys. Rev. A **15**, 227 (1977).
[26] J. L. Hall, L. Hollberg, T. Baer, and H. G. Robinson, Appl. Phys. Lett. **39**, 680 (1981).
[27] See, for example, L. Allen and J. H. Eberly, *Optical Resonance and Two-level Atoms* (Wiley, New York, 1975).